JOC The Journal of Organic Chemistry

pubs.acs.org/joc Article

N-Methylation of Self-Immolative Thiocarbamates Provides Insights into the Mechanism of Carbonyl Sulfide Release

Carolyn M. Levinn, Jenna L. Mancuso, Rachel E. Lutz, Haley M. Smith, Christopher H. Hendon, and Michael D. Pluth*

Cite This: *J. Org. Chem.* 2021, 86, 5443−5451 Read Online

ACCESS | Metrics & More | Article Recommendations | Supporting Information

ABSTRACT: Hydrogen sulfide (H_2S) is an important biomolecule, and self-immolative thiocarbamates have shown great promise as triggerable H_2S donors with suitable analogous control compounds; however, thiocarbamates with electron-deficient payloads are less efficient H_2S donors. We report here the synthesis and study of a series of *N*-methylated esterase-triggered thiocarbamates that block the postulated unproductive deprotonation-based pathway for these compounds. The relative reaction profiles for H_2S release across a series of electron-rich and electron-poor N-Me aniline payloads are examined experimentally and computationally. We show that thiocarbamate *N*-methylation does block some side reactivity and increases the H_2S release profiles for electron-poor donors. Additionally, we show that isothiocyanate release is not a competitive pathway, and rather that the reduced efficiency of electron-poor donors is likely due to other side reactions.

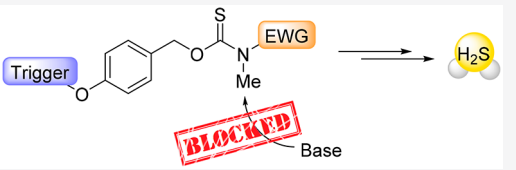

INTRODUCTION

Hydrogen sulfide (H_2S) is an important biomolecule that is involved in cardioprotection from oxidative stress associated with myocardial infarction and ischemia-reperfusion events[1,2] and that has shown promising roles in potential treatments for neurodegenerative diseases,[3,4] including Parkinson's[5] and Alzheimer's diseases.[6] Many H_2S-related investigations, however, provide conflicting activities, with H_2S having been shown to have both pro-[7] and anti-inflammatory,[8,9] as well as both pro-[10] and antiapoptotic[11,12] effects, depending on the specific study. These prior results highlight the need for a better understanding of how H_2S is delivered in different contexts and different tools to enable specific investigations. This need has led many research groups to develop a broad array of donor platforms to deliver known quantities of H_2S (or H_2S equivalents) at controllable rates and in response to specific stimuli.[13]

Rather than use H_2S directly, chemists have developed a variety of strategies to deliver H_2S in biological environments. For example, donor motifs have been developed in which hydrolysis or thiolysis results in H_2S release.[13] Alternatively, other approaches have utilized the intermediate release of carbonyl sulfide (COS), which is rapidly converted to H_2S by the enzyme carbonic anhydrase (CA) (Figure 1a).[14,15] One common platform within this approach is the use of self-immolative thiocarbamates that can be triggered by specific stimuli to release COS. Moreover, these donor motifs provide access to critical control compounds, including triggerless control compounds and sulfur-depleted control compounds that release CO_2 rather than COS. Highlighting the diversity of this platform, prior donors have been developed that respond to both external and internal stimuli, including endogenous levels of peroxide,[16,17] bio-orthogonal chemistry,[18] enzymes,[19,20] thiols,[21−23] acid,[24] nucleophiles,[25,26] and light.[27−29]

An attractive approach to tune the release rates of thiocarbamate-based donors is to modify the electron donating or withdrawing nature of the aniline payload. One would expect that more electron-deficient anilines would favor an increased rate of self-immolation by stabilizing the charge build-up on the nitrogen atom in the COS-releasing transition state.[30] In our recent investigation into esterase-triggered thiocarbamates, however, we failed to observe the expected correlation between COS/H_2S release rates and aniline σ_p values. One explanation for this divergence is that electron-withdrawing aniline payloads would acidify the thiocarbamate N−H, resulting in potential deprotonation, isothiocyanate formation, and benzyl alcohol release. This nonproductive pathway would reduce the efficiency of COS/H_2S release (Figure 1b). Consistent with this hypothesis, Chakrapani and co-workers invoked this competing deprotonation mechanism in a similar system studying *S*-alkyl thiocarbamates with aryl and benzyl amine payloads.[17,31]

To investigate this hypothesis directly, here we report a simple method for preparation of *N*-methylated thiocarbamates and assess the COS/H_2S releasing efficiency of a library

Received: November 19, 2020
Published: April 5, 2021

https://doi.org/10.1021/acs.joc.0c02778
J. Org. Chem. 2021, 86, 5443−5451

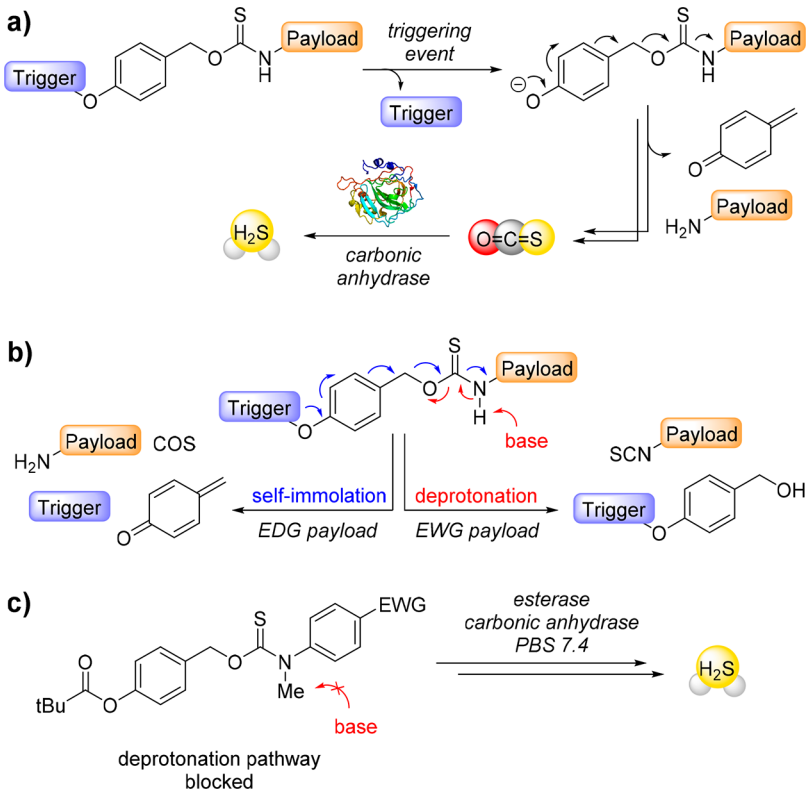

Figure 1. (a) Mechanism of COS/H_2S release from self-immolative thiocarbamates. (b) Proposed competing breakdown pathways of thiocarbamates that include self-immolative release of COS for electron-rich substrates (left, blue) and deprotonation to release an isothiocyanate (red, right) for electron-poor substrates. (c) This work: *N*-methylation of thiocarbamate blocks the potential deprotonation pathway allowing for COS-release from electron-poor substrates.

of *N*−H and *N*−Me self-immolative thiocarbamates (Figure 1c). Moreover, we provide computational insights into three possible reaction trajectories, which reveals large thermal barriers for isothiocyanate formation and supports thiocarbamate hydrolysis to thiocarbonic acid as a more likely alternative route for electron-withdrawing substituents.

RESULTS AND DISCUSSION

Many commonly used methods to prepare thiocarbamates involve the addition of an alcohol or mercaptan into an isothiocyanate or isocyanate, respectively.[30] Our initial attempts to prepare *N*-methyl thiocarbamates focused on direct methylation of the thiocarbamate nitrogen. Although this method works well for the parent carbamate compounds, similar approaches with thiocarbamates resulted in undesired alkylation of the sulfur. We were able to circumvent this problem by the addition of one equivalent of an *N*-methylated aniline into thiocarbonyldiimidazole (TCDI) to produce an asymmetric mixed thiourea. This useful intermediate coupling partner could then be further reacted with a benzyl alcohol to access the desired *N*−Me *O*-alkyl thiocarbamates. Moreover, this mixed thiourea approach provides a versatile platform for accessing differently functionalized thiocarbamates that are otherwise difficult to access through standard methods. Following this protocol, we prepared a suite of *N*−Me thiocarbamates with a range of electronically modified payloads (Figure 2).[32]

With the *N*-methylated *O*-alkyl thiocarbamate donors in hand, the COS/H_2S release profiles were measured using the colorimetric methylene blue assay.[33] We measured H_2S release

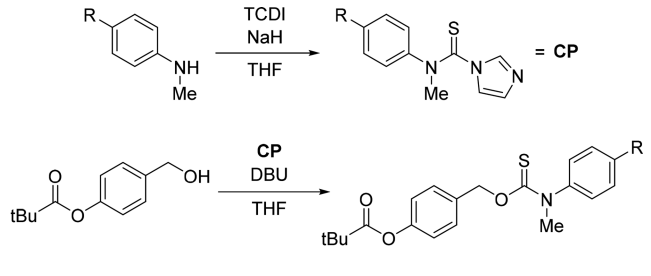

		coupling partner		thiocarbamate	
EWG	R = NO_2	CP-NO_2	26%	MeTCM-NO_2	33%
	R = CF_3	CP-CF_3	81%	MeTCM-CF_3	10%
	R = OCF_3	CP-OCF_3	60%	MeTCM-OCF_3	14%
	R = F	CP-F	55%	MeTCM-F	21%
	R = H	CP-H	75%	MeTCM-H	19%
	R = Me	CP-Me	99%	MeTCM-Me	22%
EDG	R = OMe	CP-OMe	95%	MeTCM-OMe	9%

Figure 2. Synthesis and yields of coupling partners and final *O*-alkyl *N*-methyl thiocarbamate COS/H_2S donors.

from the thiocarbamates (50 μM) in phosphate-buffered saline solutions (10 mM PBS, pH 7.4) with 2% DMSO in the presence of carbonic anhydrase (CA, 50 μg/mL) and porcine liver esterase (PLE, 5 U/mL) at 25 °C. The methylene blue aliquots were passed through a 0.2 μm syringe filter prior to absorbance measurements to remove any precipitated PLE from the acidic methylene blue solution. On the basis of the buildup of negative charge on the thiocarbamate in the proposed COS-release mechanism, as well as prior work by the

https://doi.org/10.1021/acs.joc.0c02778
J. Org. Chem. 2021, 86, 5443−5451

Chakrapani lab demonstrating an inverse relationship between N−H pK_a and H_2S release rate on *S*-alkyl thiocarbamates,[31] we hypothesized that installing electron-withdrawing substituents on the payload would lead to faster peaking times and higher overall amounts of H_2S/COS released, with the *p*-NO_2 donors being the most efficient. Accordingly, what we observed was that release from electron-rich donors peaked at the lowest concentrations of H_2S, whereas the electron-poor donors peaked at higher H_2S concentrations but with slower overall peaking times (Figure 3, Figure S42).

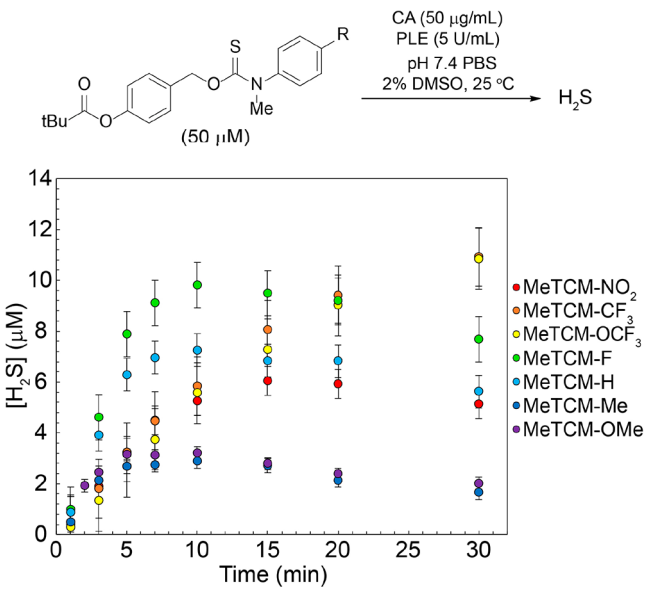

Figure 3. H_2S release profiles of *O*-alkyl *N*-methyl thiocarbamate donors. H_2S concentrations were measured using the methylene blue assay. Each experiment was performed in quadruplicate.

To directly compare the effects of the *N*-methylation on COS/H_2S release from thiocarbamates, we next measured the H_2S release from *p*-NO_2 and *p*-Me *N*−H thiocarbamate donors. We found that *N*-methylation significantly increased the observed H_2S release from the *p*-NO_2 donor relative to the parent *N*−H as predicted, while MeTCM-Me was significantly less efficient than the *N*−H donor (HTCM-Me). Interestingly, the HTCM-Me donor displayed the fastest initial rate of H_2S release under these conditions, even when compared to the MeTCM-NO_2 donor (Figure 4).

To further probe the energetics of potential competing pathways for COS/H_2S release, we used DFT investigations to directly compare how electronic modification of the different substrates influenced alternative release pathways. Using Gaussian 09,[34] we optimized the different ground state and transition state geometries for the pathways at the B3LYP/6-311++G(d,p) level of theory. Using this approach, we investigated the 1,6-self-immolation and COS extrusion pathway (Figure 5a, black) and also two additional reaction trajectories. Specifically, these included deprotonation of the thiocarbamate *N*−H to release an isothiocyanate (Figure 5a red, alternate path I), and protonation of the intermediate thiocarbamate anion formed after self-immolation and subsequent hydrolysis to form thiocarbonic acid (Figure 5a blue, alternate path II).

Along the self-immolation/COS-extrusion pathway (Figure 5, black), deprotonation of the phenol to form the phenoxide

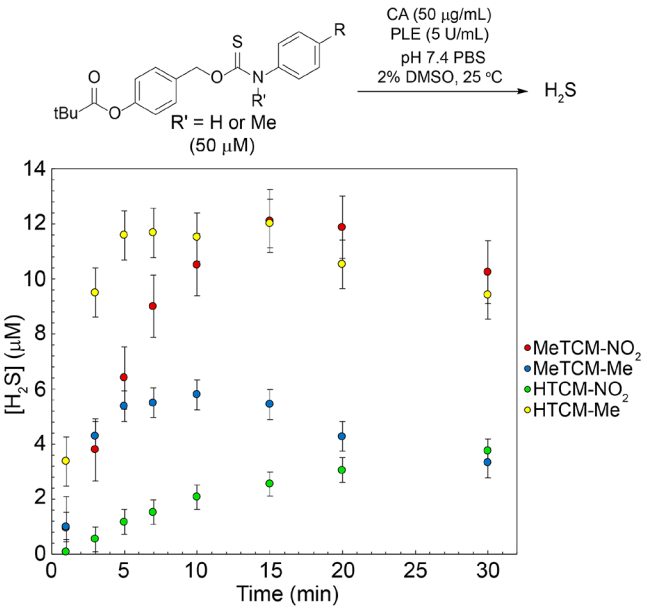

Figure 4. H_2S release profiles of select *O*-alkyl *N*-methyl and *N*−H thiocarbamate donors. H_2S concentrations were measured using the methylene blue assay. Each experiment was performed in quadruplicate.

precedes self-immolation TS1 to release a *para*-quinone methide (QM) and a thiocarbamate anion intermediate. Our computational investigations suggested that the water-assisted COS-extrusion from the thiocarbamate anion intermediate TS2 is significantly lower than the unassisted pathway. COS-extrusion through TS2 results in release of the aniline payload, which is subsequently protonated to yield an overall exergonic reaction. We note that these final energies do not account for the additional energy gain from rearomatization of the *para*-quinone methide. Alternate path I (red) follows the possible deprotonation-based reaction pathway, in which the thiocarbamate N−H is deprotonated, resulting in release of an isothiocyanate and a benzyl alkoxide, which is subsequently protonated. Lastly, we investigated alternate path II (blue) that intercepts the self-immolation pathway at the thiocarbamate anion. Instead of COS extrusion, protonation of the thiocarbamate anion to the thioacid and subsequent hydrolysis would release the same aniline payload, alongside an equivalent of thiocarbonic acid, which prior reports show can decompose to release COS and H_2O.[35]

When comparing the energy coordinate diagrams for the self-immolation pathway (Figure 5 black, *N*−H (dot) and *N*−Me (bar) donors), the relative energies of the first transition state are very similar ($\Delta\Delta G$ ~2.6 kcal/mol) for all of the donors regardless of *N*-alkylation or payload electronics. The stabilities of the resultant thiocarbamate anions, however, show significant differences with the thiocarbamate anion from HTCM-NO_2 being ~5 kcal/mol more stable than any other donor investigated. The relative energies over the second COS-releasing transition state TS2 are much more dispersed, with the *N*−Me donor intermediates on average about 3 kcal/mol higher in energy than their *N*−H counterparts. Thiocarbamate methylation was expected to reduce reaction rates due to mild electron-donation into the formally anionic pathway, which is reflected in both the experimental (Figure 4) and computational data (Figure 5b). Additionally, we hypothesize that the steric bulk of the *N*-methyl relative to

https://doi.org/10.1021/acs.joc.0c02778
J. Org. Chem. 2021, 86, 5443−5451

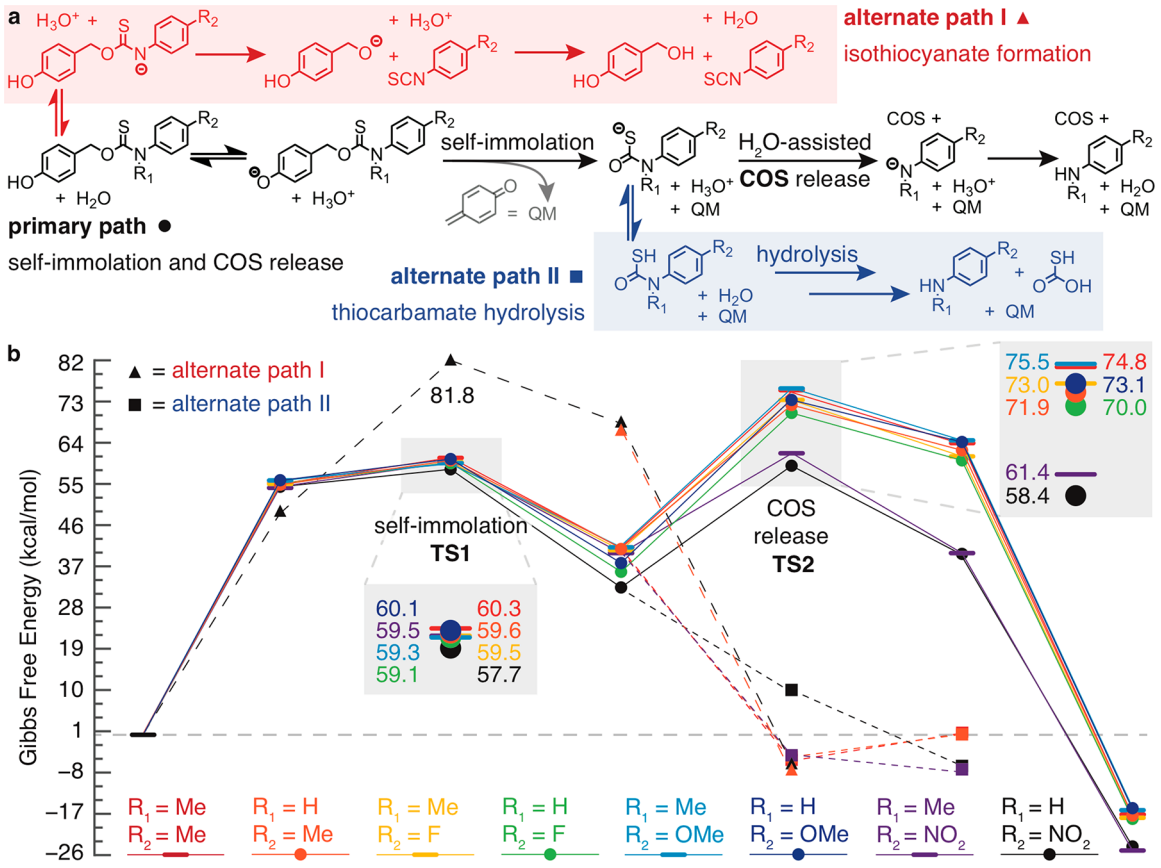

Figure 5. (a) The intended reaction pathway for thiocarbamate scaffolds where R_1 = H, Me and R_2 = Me, F, OMe, NO_2 is shown in black with alternate paths I and II shown in red/triangles and blue/squares, respectively, that were investigated computationally in this study. (b) Gibbs Free Energy coordinate diagram comparing the relative energies of each proposed reaction pathway recovered from B3LYP/6-311++G** including the PCM for water as implemented in Gaussian09.

the *N*−H has a significant effect on the conformation of the thiocarbamate, which could influence the orbital overlap between the thiocarbamate moiety and the aryl ring of the payload, impacting the rates of COS extrusion.[36]

Beyond the predictable slight electronic effects of *N*-methylation, comparing the zero-point energy corrected energy barriers for the rate-determining step of COS-release from the thiocarbamate anions we see that scaffolds with electron-donating groups in the R_2-position have higher activation barriers for COS release, whereas donors with electron-withdrawing groups in the R_2 position have lower barriers as expected. The relative barriers for the rate-determining step (TS2) for donors in which R_2 = NO_2 (MeTCM-NO_2 and HTCM-NO_2), however, indicate that they should release H_2S much more efficiently than experimentally observed. To examine whether this reduced production is the result of *N*−H acidification, we next investigated deprotonation of the *N*−H scaffold following the expected competing pathway to isothiocyanate formation (alternative path I, Figure 5b black triangles).

Deprotonation of the *N*−H in HTCM-NO_2 is favorable as expected, which is supported by the relative stability of the resulting anion compared with deprotonation of the phenol trigger, yet the activation barrier for benzyl alcohol release is over 20 kcal/mol higher than the rate-determining step for COS release (TS1), indicating that the benzyl alcohol release pathway is largely inactive. The reversible deprotonation of the acidified thiocarbamate *N*−H when R_2 = NO_2, however, still likely plays a role in the observed reduced rates of H_2S production. For HTCM-Me, deprotonation at the nitrogen and oxygen are effectively the same (54.8(6) and 54.9(2) kcal/mol, respectively) and the transition state for isothiocyanate formation could not be isolated, but would be expected to be considerably less stable than when R_2 = NO_2.

On the basis of these parameters, we expect that alternate path II (Figure 5a, blue, and Figure 5b, black squares), in which the thiocarbamate anion is protonated and subsequently hydrolyzed to reveal thiocarbonic acid, is likely a more favorable competing pathway. Consistent with this idea, prior reports have indicated that thiocarbonic acid dimer complexes can decompose to generate two equivalents of COS and H_2O,[35] which in this system would be converted to H_2S by CA. Potential energy surface scans performed to identify the activation barrier for water attack at the thiocarboxylic acid carbonyl revealed a barrierless transition (Figure S52) to higher energy zwitterionic intermediates, for which equilibrium structures could not be found, which is consistent with fast decomposition. Notably, hydrolysis to complete alternate path II is exergonic for R_2 = NO_2 scaffolds (−6.35 kcal/mol for HTCM-NO_2, −7.21 kcal/mol for MeTCM-NO_2) but slightly endergonic when R_2 = Me (0.47 kcal/mol for HTCM-Me, 0.42 kcal/mol for MeTCM-Me) (squares and small dashed lines, Figure 5b). To test this pathway experimentally, we monitored for H_2S release using the methylene blue assay from HTCM-NO_2 in the absence of CA and failed to observe significant H_2S release (Figure S47). These results suggest that if functional,

https://doi.org/10.1021/acs.joc.0c02778
J. Org. Chem. 2021, 86, 5443−5451

this pathway is not a major contributor to H_2S release over at least the first few hours of donor activation.

CONCLUSIONS

In conclusion, we have designed a platform for the synthesis of *N*-alkyl self-immolative thiocarbamate COS donors, which we have shown to have significantly different rates of H_2S release than the parent *N*−H analogues. *N*-Methylation also allows for access to thiocarbamates with electron deficient payloads, which were otherwise slow to release H_2S from the *N*−H congeners. Using computational investigations into the mechanism of COS release from *O*-alkyl thiocarbamates, we show that the isothiocyanate formation pathway is energetically disfavored. The lower levels of H_2S release from thiocarbamates with electron-withdrawing payloads are likely due to a combination of side reactions due to the acidity of the *N*−H and the reduced electrophilicity of the carbonyl in the thiocarbamate anion when compared to electron-rich systems. We anticipate these findings will help to inform researchers in future H_2S donor design and will expand the chemical space available for thiocarbamate-based COS donors.

EXPERIMENTAL SECTION

Synthesis/Spectral Details of Prepared Compounds. Reagents were purchased from Sigma-Aldrich, VWR, Acros Organics, or Tokyo Chemical Industry (TCI) and were used as received. Spectroscopic grade, inhibitor-free THF was deoxygenated by sparging with argon followed by passage through a Pure Process Technologies solvent purification system to remove water. Deuterated solvents were purchased from Cambridge Isotope Laboratories and used as received. Silica gel (SiliaFlash F60, Silicycle, 230−400 mesh) was used for column chromatography. ^{1}H, ^{13}C{^{1}H}, and ^{19}F NMR spectra were recorded on a Bruker 500 or 600 MHz instrument (as indicated). Chemical shifts are reported in parts per million relative to residual protic solvent resonances. Mass spectrometric measurements were performed by the University of Illinois, Urbana−Champaign MS facility. All air-free manipulations were performed under an inert atmosphere using standard Schlenk techniques or an Innovative Atmospheres N_2-filled glovebox. **HTCM-NO$_2$**, **HTCM-F**, and **HTCM-Me** were prepared as described in the literature, with spectral data matching those reported previously.[30]

H_2S Detection Materials and Methods. *H_2S Detection Materials and Methods.* Phosphate buffered saline (PBS) tablets (1X, CalBioChem) were used to prepare buffered solutions (140 mM NaCl, 3 mM KCl, 10 mM phosphate, pH 7.4) in deionized water. Buffer solutions were sparged with nitrogen to remove dissolved oxygen and stored in an Innovative Atmosphere nitrogen-filled glovebox. Donor stock solutions (in DMSO) were prepared inside a nitrogen-filled glovebox immediately before use. PLE stock solutions (in PBS) were freshly prepared in an N_2-filled glovebox immediately before use. CA stock solutions (in PBS) were freshly prepared in a nitrogen-filled glovebox immediately before use.

General Procedure for Measuring H_2S Release with the Methylene Blue Assay (MBA). Scintillation vials containing 20 mL of 10 mM PBS (pH 7.4) with 2% DMSO were prepared in a nitrogen-filled glovebox. To these solutions, 100 μL of 10 mg mL^{-1} CA and 50 μL of a 20 mM DMSO donor stock were added for final concentrations 50 μg mL^{-1} and 50 μM, respectively. Immediately prior to PLE addition, 0.5 mL solutions of methylene blue cocktail were prepared. The methylene blue cocktail solution contains: 200 μL of 30 mM $FeCl_3$ in 1.2 M HCl, 200 μL of 20 mM *N*,*N*-dimethyl-*p*-phenylenediamine in 7.2 M HCl, and 100 μL of 1% (w/v) $Zn(OAc)_2$. To begin an experiment, 100 μL of 1000 U/mL PLE stock solution was added for a final concentration of 5 U/mL. At set time points after the addition of PLE, 500 μL reaction aliquots were added to the methylene blue cocktail solutions and incubated for 1 h at room temperature shielded from light, then filtered through a 0.2 μm syringe filter into disposable 1.5 mL cuvettes. Absorbance values at 670 nm were measured 1 h after addition of reaction aliquot. Each experiment was performed in quadruplicate unless stated otherwise. UV/vis spectra were acquired on an Agilent Cary 60 UV/vis spectrophotometer equipped with a Quantum Northwest TC-1 temperature controller set at 25 ± 0.05 °C.

Establishing the Calibration Curve for the Methylene Blue Assay. Solutions containing 0.5 mL of methylene blue cocktail and 0.5 mL PBS (pH 7.4) containing 5% DMSO, 5 U/mL PLE, and 50 μg/mL CA were freshly prepared in disposable 1.5 mL cuvettes. Under inert conditions, a 10 mM stock solution of NaSH (Strem Chemicals) in PBS was prepared and diluted to 1 mM. Immediately after dilution, varying amounts of the 1 mM NaSH stock was added to 1.0 mL solutions for final concentrations of 10, 20, 30, 40, 50, and 60 μM. Solutions were mixed, filtered through a 0.2 μm syringe filter, incubated at room temperature for 1 h, and shielded from light. Absorbance values at 670 nm were measured after 1 h.

Computational Methods. Density functional theory (DFT) as implemented in Gaussian09[34] with the hybrid functional B3LYP and the triple-ζ Pople basis set with diffuse and polarization functions on all atoms (6-311++G(d,p)) was employed to equilibrate all intermediate and transition state structures. A superfine grid and tight convergence criteria were used for all calculations. A self-consistent reaction field was included with the dielectric constant of water using the polarizable continuum model in order to simulate the biological environment. Vibrational analysis was further performed to recover thermodynamic values, including the zero-point energy correction, and to ensure that ground state structures each had zero negative frequencies, while all activated complexes had exactly one corresponding to the appropriate bond breaking/forming reaction coordinate.

Synthetic Procedures. *General Procedure for the Synthesis of N-Me Coupling Partners. General Procedure A.* The *para*-substituted *N*−Me aniline (1.0 equiv) and TCDI (2.0 equiv) were dissolved in anhydrous THF (0.15 M solution based on aniline) in a flame-dried round-bottomed flask equipped with a magnetic stir bar under an inert N_2 atmosphere. The reaction mixture was refluxed at 70 °C in a silicone oil bath overnight, and then the solvent was removed under reduced pressure. The crude residue was dissolved in EtOAc, quenched with brine, and extracted with EtOAc (3 × 20 mL). The combined organic layers were dried over anhydrous $MgSO_4$ and purified via silica column chromatography (1:1 Hex:EtOAc).

General Procedure B. The *para*-substituted *N*−Me aniline (1.0 equiv) and TCDI (1.2 equiv) were dissolved in anhydrous THF (0.1 M solution based on aniline) and cooled to 0 °C in an ice bath under an inert N_2 atmosphere. NaH (1.1 equiv) was added, and the reaction mixture was allowed to slowly warm to room temperature and stir overnight. The reaction mixture was quenched with brine, extracted with EtOAc (3 × 20 mL), and the combined organic layers were dried over anhydrous $MgSO_4$ and purified via silica column chromatography (1:1 Hex:EtOAc).

CP-OMe was prepared with 4-methoxy-*N*-methylaniline and TCDI according to the general procedure A and purified by column chromatography (1:1 Hex:EtOAc) as described above. (reddish-brown solid, 856 mg, 95% yield). ^{1}H NMR (600 MHz, $CDCl_3$) δ (ppm) 7.69 (t, *J* = 1.02 Hz, 1H), 6.96 (m, 3H), 6.82 (m, 2H), 6.77 (dd, *J* = 1.02, 1.61 Hz, 1H), 3.81 (s, 3H), 3.76 (s, 3H). ^{13}C{^{1}H} NMR (151 MHz, $CDCl_3$) δ (ppm) 178.5, 158.9, 137.9, 137.7, 129.0, 125.7, 119.9, 115.3, 55.5, 47.2. IR (cm^{-1}) 3462, 3147, 3003, 2970, 2362, 1739, 1604, 1584, 1524, 1504, 1472, 1459, 1364, 1312, 1288, 1228, 1217, 1168, 1127, 1104, 1092, 1066, 1036, 1015, 1006, 910. HRMS *m*/*z* [M + H]$^+$ calcd. for $[C_{12}H_{14}N_3OS]^+$ 248.0858, found 248.0852.

CP-Me was prepared with 4-methyl-*N*-methylaniline and TCDI according to the general procedure A and purified by column chromatography (1:1 Hex:EtOAc) as described above. (off-white solid, 378 mg, 99% yield). ^{1}H NMR (500 MHz, $CDCl_3$) δ (ppm) 7.65 (t, *J* = 0.94 Hz, 1H), 7.11 (d, *J* = 8.34 Hz, 2H), 6.98 (t, *J* = 1.49 Hz, 1H), 6.92 (d, *J* = 8.34 Hz, 2H), 6.76 (dd, *J* = 0.94, 1.49 Hz, 1H), 3.81 (s, 3H), 2.30 (s, 3H). ^{13}C{^{1}H} NMR (126 MHz, $CDCl_3$) δ

https://doi.org/10.1021/acs.joc.0c02778
J. Org. Chem. 2021, 86, 5443−5451

(ppm) 178.5, 142.5, 138.3, 137.8, 130.7, 129.0, 124.3, 120.0, 47.0. IR (cm^{-1}) 3162, 2922, 1738, 1507, 1524, 1481, 1456, 1389, 1364, 1296, 1268, 1255, 1217, 1125, 1108, 1094, 1062, 1013, 912. HRMS *m/z* $[M + H]^+$ calcd. for $[C_{12}H_{14}N_3S]^+$ 232.0908, found 232.0903.

CP-H was prepared with *N*-methylaniline and TCDI according to the general procedure A and purified by column chromatography (1:1 Hex:EtOAc) as described above. (colorless oil, 606 mg, 75% yield). ^1H NMR (600 MHz, $CDCl_3$) δ (ppm) 7.69 (t, J = 1.0 Hz, 2H), 7.33 (m, 2H), 7.27 (m, 1H), 7.05 (m, 2H), 6.96 (t, J = 1.48 Hz, 1H), 6.76 (dd, J = 1.0, 1.48 Hz, 1H), 3.84 (s, 3H). $^{13}C\{^1H\}$ NMR (151 MHz, $CDCl_3$) δ (ppm) 178.6, 145.0, 137.9, 130.2, 129.1, 128.1, 124.6, 119.9, 46.9. IR (cm^{-1}) 3118, 2913, 1593, 1518, 1491, 1466, 1382, 1359, 1293, 1221, 1177, 1117, 1096, 1071, 1018, 1001, 917. HRMS *m/z* $[M + H]^+$ calcd. for $[C_{11}H_{12}N_3S]^+$ 218.0752, found 218.0744.

CP-F was prepared with 4-fluoro-*N*-methylaniline and TCDI according to the general procedure A and purified by column chromatography (1:1 Hex:EtOAc) as described above. (pale yellow solid, 1.04 g, 55% yield). ^1H NMR (600 MHz, $CDCl_3$) δ (ppm) 7.69 (t, J = 1.01 Hz, 1H), 7.06−7.01 (m, 4H), 6.95 (t, J = 1.49 Hz, 1H), 6.80 (dd, J = 1.01, 1.49 Hz, 1H), 3.81 (s, 3H). $^{13}C\{^1H\}$ NMR (151 MHz, $CDCl_3$) δ (ppm) 178.9, 161.5 (d, C−F, $^1J_{C-F}$ = 250.4 Hz), 160.7, 141.0 (d, C−F, $^4J_{C-F}$ = 3.4 Hz), 137.8, 129.3, 126.4 (d, C−F, $^3J_{C-F}$ = 8.8 Hz), 119.8, 117.3 (d, C−F, $^2J_{C-F}$ = 22.9 Hz), 47.0. ^{19}F NMR (525 MHz, $CDCl_3$) δ (ppm) −111.7 (m). IR (cm^{-1}) 3456, 3016, 2970, 2945, 2362, 2343, 2131, 1739, 1504, 1435, 1365, 1303, 1283, 1228, 1217, 1157, 1095, 1073, 1019, 939, 914. HRMS *m/z* $[M + H]^+$ calcd. for $[C_{11}H_{11}N_3SF]^+$ 236.0658, found 236.0651.

CP-OCF$_3$ was prepared with 4-trifluoromethoxy-*N*-methylaniline and TCDI according to the general procedure A and purified by column chromatography (1:1 Hex:EtOAc) as described above. (yellow oil, 532 mg, 60% yield). ^1H NMR (600 MHz, $CDCl_3$) δ (ppm) 7.72 (bs, 1H), 7.18 (d, J = 8.94 Hz, 2H), 7.10 (d, J = 8.94 Hz, 2H), 6.94 (bs, 1H), 6.80 (bs, 1H), 3.82 (s, 3H). $^{13}C\{^1H\}$ NMR (151 MHz, $CDCl_3$) δ (ppm) 178.8, 148.16 (q, C−F, $^3J_{C-F}$ = 1.6 Hz), 143.3, 137.8, 129.5, 126.2, 122.5, 121.1 (q, C−F, $^1J_{C-F}$ = 257.6 Hz), 119.7, 46.8. ^{19}F NMR (525 MHz, $CDCl_3$) δ (ppm) −58.0 (bs). IR (cm^{-1}) 3115, 1501, 1468, 1383, 1363, 1249, 1203, 1159, 1118, 1096, 1015, 919. HRMS *m/z* $[M + H]^+$ calcd. for $[C_{12}H_{11}F_3N_3OS]^+$ 302.0575, found 302.0565.

CP-CF$_3$ was prepared with 4-trifluoromethyl-*N*-methylaniline and TCDI according to the general procedure B and purified by column chromatography (1:1 Hex:EtOAc) as described above. (yellow oil, 625 mg, 81% yield). ^1H NMR (600 MHz, $CDCl_3$) δ (ppm) 7.69 (d, J = 1.0 Hz, 1H), 7.60 (d, J = 8.88 Hz, 2H), 7.18 (d, J = 8.88 Hz, 2H), 6.96 (t, J = 1.50 Hz, 1H), 6.80 (dd, J = 1.0, 1.50 Hz, 1H), 3.84 (s, 3H). $^{13}C\{^1H\}$ NMR (151 MHz, $CDCl_3$) δ (ppm) 178.9, 148.0 (q, C−F, $^4J_{C-F}$ = 1.3 Hz), 137.7, 129.8 (q, C−F, $^2J_{C-F}$ = 33.3 Hz), 129.7, 127.4 (q, C−F, $^3J_{C-F}$ = 3.8 Hz), 125.0, 123.2 (q, C−F, $^1J_{C-F}$ = 272.3 Hz), 119.7, 46.6. ^{19}F NMR (565 MHz, $CDCl_3$) δ (ppm) −63.7. IR (cm^{-1}) 3113, 1614, 1590, 1515, 1466, 1417, 1388, 1361, 1320, 1301, 1285, 1253, 1223, 1165, 1117, 1096, 1062, 1014, 954, 919. HRMS *m/z* $[M + H]^+$ calcd. for $[C_{12}H_{11}N_3F_3S]^+$ 286.0626, found 286.0616.

CP-NO$_2$ was prepared with 4-nitro-*N*-methylaniline and TCDI according to the general procedure B and purified by column chromatography (1:1 Hex:EtOAc) as described above. (40 mg yellow solid, 26% yield). ^1H NMR (600 MHz, $CDCl_3$) δ (ppm) 8.16 (d, J = 8.97 Hz, 2H), 7.67 (t, J = 1.08 Hz, 1H), 7.21 (d, J = 8.97 Hz, 2H), 6.95 (t, J = 1.44 Hz, 1H), 6.80 (dd, J = 1.08, 1.44 Hz, 1H), 3.83 (s, 3H). $^{13}C\{^1H\}$ NMR (151 MHz, $CDCl_3$) δ (ppm) 178.9, 150.3, 146.2, 137.6, 130.0, 125.6, 125.4, 119.7, 46.4. IR (cm^{-1}) 3460, 3132, 3071, 3016, 2970, 2944, 2360, 2128, 1739, 1607, 1591, 1515, 1487, 1456, 1366, 1304, 1285, 1227, 1217, 1122, 1104, 1073, 1017, 1009, 919. HRMS *m/z* $[M + H]^+$ calcd. for $[C_{11}H_{11}N_4O_2S]^+$ 263.0603, found 263.0604.

General Procedure for the Synthesis of N-Methyl Thiocarbamates. 4-(Hydroxymethyl)phenyl pivalate was prepared according to the literature procedure.[37] 4-(Hydroxymethyl)phenyl pivalate (1.0 equiv) and an *N*−Me coupling partner (5.0 equiv) were dissolved in anhydrous THF (0.1 M solution) and put under an atmosphere of N_2. DBU (1.2 equiv) was added, and the reaction mixture was stirred, heated to 40 °C in a silicone oil bath, and monitored by TLC. Upon completion, the reaction mixture was quenched with brine, extracted with EtOAc (3 × 10 mL), the combined organic layers were dried over anhydrous $MgSO_4$, and the crude product purified by silica gel column chromatography (10:1 Hexanes:EtOAc). Unreacted coupling partner was also isolated and purified.

MeTCM-OMe was prepared with CP-OMe and 4-(hydroxymethyl)phenyl pivalate according to the general procedure as described above and purified by column chromatography (10:1 Hex:EtOAc) (24 mg, 9% yield, off-white solid). ^1H NMR (600 MHz, DMSO-d_6, 60 °C) δ (ppm) 7.36−6.82 (m, 8H), 5.47 (bs, 2H), 3.78 (s, 3H), 3.55 (bs, 3H), 1.31 (s, 9H). $^{13}C\{^1H\}$ NMR (151 MHz, DMSO-d_6, 60 °C) δ (ppm) 188.4, 176.7, 170.7, 158.7, 150.9, 134.0, 129.0, 129.0, 128.9, 127.4, 121.9, 114.9, 71.9, 60.1, 55.9, 55.3 39.0, 27.2, 21.2, 14.5. IR (cm^{-1}) 2969, 2930, 2359, 1748, 1608, 1509, 1478, 1383, 1277, 1246, 1194, 1164, 1112, 1030, 941. HRMS *m/z* $[M + H]^+$ calcd. for $[C_{21}H_{26}NO_4S]^+$ 388.1583, found 388.1579.

MeTCM-Me was prepared with CP-Me and 4-(hydroxymethyl)-phenyl pivalate according to the general procedure as described above and purified by column chromatography (10:1 Hex:EtOAc) (white solid, 62 mg, 22% yield). ^1H NMR (500 MHz, DMSO-d_6, 60 °C) δ (ppm) 7.55−6.83 (m, 8H), 5.48 (s, 2H), 3.54 (bs, 3H), 2.33 (s, 3H), 1.31 (s, 9H). $^{13}C\{^1H\}$ NMR (151 MHz, DMSO-d_6, 60 °C) δ (ppm) 188.2, 176.7, 150.9, 137.2, 133.9, 130.1, 129.0, 122.1, 121.9, 71.9, 55.3, 39.0, 27.4, 27.2, 21.0. IR (cm^{-1}) 3456, 3016, 2970, 2361, 1739, 1435, 1366, 1229, 1217, 1113. HRMS *m/z* $[M + H]^+$ calcd. for $[C_{21}H_{26}NO_3S]^+$ 372.1633, found 372.1627.

MeTCM-H was prepared with CP-H and 4-(hydroxymethyl)-phenyl pivalate according to the general procedure as described above and purified by column chromatography (10:1 Hex:EtOAc) (colorless oil, 50 mg, 19% yield). ^1H NMR (500 MHz, DMSO-d_6, 60 °C) δ (ppm) 7.49−7.20 (m, 7H), 7.04 (d, J = 8.03 Hz, 2H), 5.47 (s, 2H), 3.56 (s, 3H), 1.31 (s, 9H). $^{13}C\{^1H\}$ NMR (151 MHz, DMSO-d_6, 60 °C) δ (ppm) 188.3, 176.7, 150.9, 133.9, 129.6, 129.0, 127.8, 126.6, 121.9, 72.0, 39.0, 27.2. IR (cm^{-1}) 2970, 2933, 2875, 2360, 1748, 1594, 1494, 1462, 1384, 1364, 1277, 1229, 1213, 1189, 1163, 1151, 1112, 1029, 1017, 1005, 994, 944. HRMS *m/z* $[M + H]^+$ calcd. for $[C_{20}H_{24}NO_3S]^+$ 358.1477, found 358.1476.

MeTCM-F was prepared with CP-F and 4-(hydroxymethyl)phenyl pivalate according to the general procedure as described above and purified by column chromatography (10:1 Hex:EtOAc) (colorless oil, 51 mg, 21% yield). ^1H NMR (500 MHz, DMSO-d_6, 60 °C) δ (ppm) 7.47−7.14 (m, 6H), 7.06 (d, J = 7.99 Hz, 2H), 5.48 (s, 2H), 3.54 (s, 3H), 1.31 (s, 9H). $^{13}C\{^1H\}$ NMR (151 MHz, DMSO-d_6, 60 °C) δ (ppm) 188.5, 176.7, 161.2 (d, C−F, $^1J_{C-F}$ = 244.8 Hz), 151.0, 133.8, 130.5, 129.8, 129.1, 128.8, 122.1, 122.0, 116.4 (d, C−F, $^2J_{C-F}$ = 22.6 Hz), 72.1, 55.2, 39.0, 27.2. ^{19}F NMR (565 MHz, DMSO-d_6, 60 °C) δ (ppm) −114.6 (m). IR (cm^{-1}) 3462, 2970, 2362, 1744, 1604, 1507, 1476, 1366, 1276, 1217, 1164, 1108, 1029, 1015, 940. HRMS *m/z* $[M + H]^+$ calcd. for $[C_{20}H_{23}NO_3FS]^+$ 376.1383, found 376.1380.

MeTCM-OCF$_3$ was prepared with CP-OCF$_3$ and 4-(hydroxymethyl)phenyl pivalate according to the general procedure as described above and purified by column chromatography (10:1 Hex:EtOAc) (colorless oil, 42 mg, 14% yield). ^1H NMR (500 MHz, DMSO-d_6, 60 °C) δ (ppm) 7.46 (d, J = 9.01 Hz, 2H), 7.40 (m, 2H), 7.30 (bs, 2H), 7.05 (d, J = 9.20 Hz, 2H), 5.49 (s, 2H), 3.56 (s, 3H), 1.31 (s, 9H). $^{13}C\{^1H\}$ NMR (126 MHz, DMSO-d_6, 60 °C) δ (ppm) 188.4, 176.7, 151.0, 147.5, 133.7, 129.2, 129.0 (q, C−F, $^1J_{C-F}$ = 248.6 Hz), 122.1, 121.9, 121.4, 119.7, 72.2, 55.3, 39.0, 27.4. ^{19}F NMR (565 MHz, DMSO-d_6, 60 °C) δ (ppm) −56.9 (s). IR (cm^{-1}) 3457, 2970, 2362, 2342, 1737, 1609, 1508, 1479, 1456, 1366, 1257, 1228, 1217, 1146, 1108, 1029, 1017, 939. HRMS *m/z* $[M + H]^+$ calcd. for $[C_{21}H_{23}NO_4F_3S]^+$ 442.1300, found 442.1297.

MeTCM-CF$_3$ was prepared with CP-CF$_3$ and 4-(hydroxymethyl)-phenyl pivalate according to the general procedure as described above and purified by column chromatography (10:1 Hex:EtOAc) (colorless oil, 30 mg, 10% yield). ^1H NMR (600 MHz, DMSO-d_6, 60 °C) δ (ppm) 7.79 (d, J = 8.25 Hz, 2H), 7.57 (d, J = 8.25 Hz, 2H), 7.33 (d, J = 8.52 Hz, 2H), 7.06 (d, J = 8.52 Hz, 2H), 5.51 (s, 2H), 3.58 (s, 3H), 1.31 (s, 9H). $^{13}C\{^1H\}$ NMR (126 MHz, DMSO-d_6, 60 °C) δ (ppm)

https://doi.org/10.1021/acs.joc.0c02778
J. Org. Chem. 2021, 86, 5443−5451

188.4, 176.7, 151.0, 133.6, 133.6, 129.8, 129.3, 129.1, 127.9, 126.7, 126.7, (q, C−F, $^{1}J_{C-F}$ = 246.4 Hz), 122.1 (m, unresolvable C−F coupling from rotamers), 72.3, 39.0, 27.2. ^{19}F NMR (565 MHz, DMSO-d_6, 60 °C) δ (ppm) −61.0. IR (cm^{-1}) 2972, 2362, 1749, 1514, 1509, 1479, 1380, 1324, 1277, 1197, 1165, 1113, 1067, 1019. HRMS m/z [M + H]$^+$ calcd. for [$C_{21}H_{23}NO_3SF_3$]$^+$ 426.1351, found 426.1343.

MeTCM-NO$_2$ was prepared with CP-NO$_2$ and 4-(hydroxymethyl)-phenyl pivalate according to the general procedure as described above and purified by column chromatography (10:1 Hex:EtOAc) (white solid, 46 mg, 33% yield). ^{1}H NMR (600 MHz, DMSO-d_6, 60 °C) δ (ppm) 8.26 (d, J = 8.96 Hz, 2H), 7.64 (d, J = 8.96 Hz, 2H), 7.35 (d, J = 8.35 Hz, 2H), 7.08 (d, J = 8.35 Hz, 2H), 5.52 (s, 2H), 3.60 (s, 3H), 1.31 (s, 9H). ^{13}C{^{1}H} NMR (126 MHz, DMSO-d_6, 60 °C) δ (ppm) 188.4, 176.7, 151.1, 149.9, 146.4, 133.4, 129.4, 128.2, 124.9, 122.0, 72.5, 42.8, 39.0, 27.2. IR (cm^{-1}) 3388, 2974, 2361, 1748, 1607.82, 1595, 1522, 1493, 1475, 1445, 1379, 1343, 1309, 1276, 1195, 1165, 1112, 1029, 1013. HRMS m/z [M + Na]$^+$ calcd. for [$C_{20}H_{22}N_2O_5SNa$]$^+$ 425.1147, found 425.1133.

S-Alkyl CP. *N*−Me *p*-toluidine (1.04 mL, 8.25 mmol, 1.0 equiv) was added dropwise to a stirring solution of CDI (2.68 g, 16.50 mmol, 2.0 equiv) dissolved in anhydrous THF (83 mL, 0.1 M solution) under an atmosphere of N$_2$. The resulting solution was heated to reflux in a silicone oil bath overnight. The reaction mixture was cooled to room temperature, and the solvent was removed under a vacuum. The remaining residue was dissolved in DCM, washed with water, dried over anhydrous MgSO$_4$, and concentrated to an off-white solid. The crude product was taken forward without further purification (1.65 g, 92% yield, white solid). ^{1}H NMR (500 MHz, CDCl$_3$) δ (ppm) 7.60 (bs, 1H), 7.18 (d, J = 8.14, 2H), 7.01 (d, J = 8.14, 2H), 6.91 (bs, 1H), 6.85 (bs, 1H), 3.47 (s, 3H), 2.35 (s, 3H). ^{13}C{^{1}H} NMR (125 MHz, CDCl$_3$) δ (ppm) 150.0, 140.2, 138.4, 137.5, 131.0, 128.3, 128.1, 125.7, 118.7, 40.3, 21.1. The unactivated coupling partner (2.62 g, 12.2 mmol, 1.0 equiv) was dissolved in anhydrous MeCN (61 mL, 0.2 M solution) and put under an atmosphere of N$_2$. MeI (3.03 mL, 48.7 mmol, 4.0 equiv) was added dropwise, and the reaction mixture was heated to reflux in a silicone oil bath with magnetic stirring overnight. Upon completion, the reaction mixture was let cool and the solvent removed via rotary evaporation, to afford the crude product, which was used with no further purification (4.2 g crude dark reddish-brown solid, 97%). ^{1}H NMR (500 MHz, CDCl$_3$) δ (ppm) 9.76 (bs, 1H), 7.50 (s, 1H), 7.38 (d, J = 8.19, 2H), 7.26 (d, J = 8.19, 2H), 7.03 (bs, 1H), 4.13 (s, 3H), 3.53 (s, 3H), 2.4 (s, 3H). ^{13}C{^{1}H} NMR (126 MHz, CDCl$_3$) δ (ppm) 171.1, 145.9, 139.7, 138.4, 137.9, 131.4, 126.4, 123.6, 121.2, 60.4, 53.5, 41.3, 38.2, 21.2, 21.0, 14.2. IR (cm^{-1}) 3438, 3043, 1723, 1642, 1580, 1532, 1509, 1410, 1365, 1304, 1268, 1145, 1109, 1045, 1016, 983, 948. HRMS m/z [M]$^+$ calcd. for [$C_{13}H_{16}N_3O$]$^+$ 230.1293, found 230.1299.

S-Alkyl MeTCM-Me. 4-(Mercaptomethyl)phenyl pivalate (40 mg, 0.18 mmol, 1.0 equiv) was added to a stirring solution of the S-alkyl CP (70.1 mg, 0.20 mmol, 1.1 equiv) in anhydrous DCM (2 mL, 0.1 M solution). Et$_3$N (30 μL, 0.21 mmol, 1.2 equiv) was added, and the reaction mixture was stirred at room temperature for 8 h. The crude reaction mixture was directly concentrated onto silica and purified via silica gel column chromatography (4:1 Hex:EtOAc) to afford the product as a white solid (43 mg, 65% yield, white solid). ^{1}H NMR (500 MHz, CDCl$_3$, 25 °C) δ (ppm) 7.29 (d, J = 8.52, 2H), 7.19 (d, J = 8.20, 2H), 7.14 (d, J = 8.20, 2H), 6.94 (d, J = 8.52, 2H), 4.06 (s, 2H), 3.31 (s, 3H), 2.37 (s, 3H), 1.34 (s, 9H). ^{13}C{^{1}H} NMR (125 MHz, CDCl$_3$) δ (ppm) 177.0, 168.4, 150.0, 135.7, 130.1, 130.0, 128.1, 121.4, 39.1, 38.4, 34.9, 27.1, 21.2. IR (cm^{-1}) 3457, 3016, 2970, 2143, 1653, 1506, 1455, 1366, 1277, 1205, 1168, 1115, 1022, 901. HRMS m/z [M + H]$^+$ calcd. for [$C_{21}H_{26}NO_3S$]$^+$ 372.1633, found 372.1634.

F-Indoline-CP. 5-fluoroindoline (500 mg, 3.65 mmol, 1.0 equiv) was added to a stirring solution of TCDI (1.30 g, 7.29 mmol, 2.0 equiv) in THF (0.1 M) under an atmosphere of N$_2$. The reaction mixture was heated at 50 °C in overnight in a silicone oil bath, cooled to room temperature, quenched with brine, and extracted with EtOAc. The combined organic layers were washed with brine, dried over anhydrous MgSO$_4$, and the solvent removed under a vacuum. The crude product was purified via silica gel column chromatography (4:1 Hex:EtOAc) to yield 529 mg (59%) of the F-indoline-CP as a yellow solid. ^{1}H NMR (500 MHz, CDCl$_3$, 25 °C) δ (ppm) 8.04 (bs, 1H), 7.18 (s, 1H), 7.13 (s, 1H), 6.93 (d, J = 7.74 Hz, 1H), 6.68 (t, J = 8.63 Hz, 1H), 6.08 (bs, 1H), 4.42 (t, J = 7.93 Hz, 2H), 3.16 (t, J = 7.93 Hz, 2H). ^{13}C{^{1}H} NMR (125 MHz, CDCl$_3$) δ (ppm) 171.7, 160.3 (d, C−F, $^{1}J_{C-F}$= 246.7 Hz), 137.4 (d, C−F $^{3}J_{C-F}$ = 2.8 Hz), 136.9 (d, C−F, $^{3}J_{C-F}$= 9.1 Hz), 128.7, 118.9, 116.8, 114.6 (d, C−F, $^{2}J_{C-F}$ = 24.0 Hz), 113.3 (d, C−F, $^{2}J_{C-F}$ = 24.0 Hz), 57.6, 27.3. ^{19}F NMR (471 MHz, CDCl$_3$, 25 °C) δ (ppm) 114.8 (s). HRMS m/z [M + H]$^+$ calcd. for [$C_{12}H_{11}N_3FS$]$^+$ 248.0658, found 248.0664.

F-Indoline-TCM. To a stirring solution of F-indoline-CP (529 mg, 2.14 mmol, 1.0 equiv) in THF (0.1 M) at 0 °C was added 4-(hydroxymethyl)phenyl pivalate (89 mg, 0.43 mmol, 0.2 equiv) and DBU (80 μL, 0.54 mmol, 0.25 equiv). The reaction mixture was stirred for 3 h while warming to room temperature, quenched with brine, and extracted with EtOAc. The combined organic layers were dried over anhydrous MgSO$_4$. The crude mixture was concentrated and purified via silica column chromatography (8:1 Hex:EtOAc) to yield F-indoline-TCM as a white solid (29.0 mg, 17% yield). ^{1}H NMR (600 MHz, DMSO-d_6, 60 °C) δ (ppm) 7.62 (bs, 1H), 7.54 (d, J = 7.93 Hz, 2H), 7.17 (bs, 1H), 7.14 (d, J = 7.93 Hz, 2H), 6.96 (bs, 1H), 5.69 (bs, 2H), 4.34 (t, J = 8.30 Hz, 2H), 3.15 (m, 2H), 1.32 (s, 9H). ^{13}C{^{1}H} NMR (151 MHz, DMSO-d_6, 60 °C) δ (ppm) 180.0, 176.7, 159.4 (d, C−F, $^{1}J_{C-F}$ = 240.0 Hz), 151.2, 137.8, 137.1, 133.6, 130.1, 129.2, 122.2, 118.3, 114.0 (d, C−F, $^{2}J_{C-F}$ = 25.0 Hz), 113.2 (d, C−F, $^{2}J_{C-F}$ = 22.3 Hz), 72.2, 54.8, 39.0, 27.2, 26.7. ^{19}F NMR (565 MHz, DMSO-d_6, 60 °C) δ (ppm) −118.5 (bs). HRMS m/z [M + H]$^+$ calcd. for [$C_{21}H_{23}FNO_3S$]$^+$ 388.1383, found 388.1376.

■ ASSOCIATED CONTENT

Supporting Information

The Supporting Information is available free of charge at https://pubs.acs.org/doi/10.1021/acs.joc.0c02778.

NMR spectra, methylene blue data, computational data (PDF)

■ AUTHOR INFORMATION

Corresponding Author

Michael D. Pluth − *Department of Chemistry and Biochemistry, Materials Science Institute, Knight Campus for Accelerating Scientific Impact, Institute of Molecular Biology, University of Oregon, Eugene, Oregon 97403, United States;* orcid.org/0000-0003-3604-653X; Email: pluth@uoregon.edu

Authors

Carolyn M. Levinn − *Department of Chemistry and Biochemistry, Materials Science Institute, Knight Campus for Accelerating Scientific Impact, Institute of Molecular Biology, University of Oregon, Eugene, Oregon 97403, United States;* orcid.org/0000-0001-7857-7465

Jenna L. Mancuso − *Department of Chemistry and Biochemistry, Materials Science Institute, Knight Campus for Accelerating Scientific Impact, Institute of Molecular Biology, University of Oregon, Eugene, Oregon 97403, United States*

Rachel E. Lutz − *Department of Chemistry and Biochemistry, Materials Science Institute, Knight Campus for Accelerating Scientific Impact, Institute of Molecular Biology, University of Oregon, Eugene, Oregon 97403, United States*

Haley M. Smith − *Department of Chemistry and Biochemistry, Materials Science Institute, Knight Campus for Accelerating Scientific Impact, Institute of Molecular Biology, University of Oregon, Eugene, Oregon 97403, United States*

https://doi.org/10.1021/acs.joc.0c02778
J. Org. Chem. 2021, 86, 5443−5451

Christopher H. Hendon − *Department of Chemistry and Biochemistry, Materials Science Institute, Knight Campus for Accelerating Scientific Impact, Institute of Molecular Biology, University of Oregon, Eugene, Oregon 97403, United States;* orcid.org/0000-0002-7132-768X

Complete contact information is available at: https://pubs.acs.org/10.1021/acs.joc.0c02778

Notes

The authors declare no competing financial interest.

■ ACKNOWLEDGMENTS

Work described in this manuscript was supported by the NIH (MDP; R01GM113030) and the NSF/GRFP (CML; DGE-1309047). We thank Kaylin Fosnacht for assistance with analysis of different compounds.

■ REFERENCES

(1) Szabo, G.; Veres, G.; Radovits, T.; Gero, D.; Modis, K.; Miesel-Groschel, C.; Horkay, F.; Karck, M.; Szabo, C. Cardioprotective effects of hydrogen sulfide. *Nitric Oxide* **2011**, *25* (2), 201−210.

(2) Donnarumma, E.; Trivedi, R. K.; Lefer, D. J. Protective Actions of H_2S in Acute Myocardial Infarction and Heart Failure. *Comp. Physiol.* **2017**, *7* (2), 583−602.

(3) Gong, Q. H.; Shi, X. R.; Hong, Z. Y.; Pan, L. L.; Liu, X. H.; Zhu, Y. Z. A New Hope for Neurodegeneration: Possible Role of Hydrogen Sulfide. *J. Alzheimer's Dis.* **2011**, *24*, 173−182.

(4) Panthi, S.; Manandhar, S.; Gautam, K. Hydrogen sulfide, nitric oxide, and neurodegenerative disorders. *Transl. Neurodegener.* **2018**, *7*, 3.

(5) Hu, L. F.; Lu, M.; Tiong, C. X.; Dawe, G. S.; Hu, G.; Bian, J. S. Neuroprotective effects of hydrogen sulfide on Parkinson's disease rat models. *Aging Cell* **2010**, *9* (2), 135−146.

(6) Vandini, E.; Ottani, A.; Zaffe, D.; Calevro, A.; Canalini, F.; Cavallini, G. M.; Rossi, R.; Guarini, S.; Giuliani, D. Mechanisms of Hydrogen Sulfide against the Progression of Severe Alzheimer's Disease in Transgenic Mice at Different Ages. *Pharmacology* **2019**, *103* (1−2), 50−60.

(7) Muniraj, N.; Stamp, L. K.; Badiei, A.; Hegde, A.; Cameron, V.; Bhatia, M. Hydrogen sulfide acts as a pro-inflammatory mediator in rheumatic disease. *Int. J. Rheum. Dis.* **2017**, *20* (2), 182−189.

(8) Benedetti, F.; Curreli, S.; Krishnan, S.; Davinelli, S.; Cocchi, F.; Scapagnini, G.; Gallo, R. C.; Zella, D. Anti-inflammatory effects of H2S during acute bacterial infection: a review. *J. Transl. Med.* **2017**, *15*, 100.

(9) Whiteman, M.; Winyard, P. G Hydrogen sulfide and inflammation: the good, thebad, the ugly and the promising. *Expert Rev. Clin. Pharmacol.* **2011**, *4*, 13−32.

(10) Yang, G.; Wu, L. Y.; Wang, R. Pro-apoptotic effect of endogenous H2S on human aorta smooth muscle cells. *FASEB J.* **2006**, *20* (1), 553−555.

(11) Shi, S.; Li, Q. S.; Li, H.; Zhang, L.; Xu, M.; Cheng, J. L.; Peng, C. H.; Xu, C. Q.; Tian, Y. Anti-apoptotic action of hydrogen sulfide is associated with early JNK inhibition. *Cell Biol. Int.* **2009**, *33* (10), 1095−1101.

(12) Zheng, D.; Chen, Z.; Chen, J. F.; Zhuang, X. M.; Feng, J. Q.; Li, J. Exogenous hydrogen sulfide exerts proliferation, anti-apoptosis, migration effects and accelerates cell cycle progression in multiple myeloma cells via activating the Akt pathway. *Oncol. Rep.* **2016**, *36* (4), 1909−1916.

(13) Levinn, C. M.; Cerda, M. M.; Pluth, M. D. Activatable Small-Molecule Hydrogen Sulfide Donors. *Antioxid. Redox Signaling* **2020**, *32* (2), 96−109.

(14) Steiger, A. K.; Zhao, Y.; Pluth, M. D. Emerging Roles of Carbonyl Sulfide in Chemical Biology: Sulfide Transporter or Gasotransmitter? *Antioxid. Redox Signaling* **2018**, *28* (16), 1516−1532.

(15) Levinn, C. M.; Cerda, M. M.; Pluth, M. D. Development and Application of Carbonyl Sulfide-Based Donors for H_2S Delivery. *Acc. Chem. Res.* **2019**, *52* (9), 2723−2731.

(16) Zhao, Y.; Pluth, M. D. Hydrogen Sulfide Donors Activated by Reactive Oxygen Species. *Angew. Chem., Int. Ed.* **2016**, *55* (47), 14638−14642.

(17) Zhao, Y.; Henthorn, H. A.; Pluth, M. D. Kinetic Insights into Hydrogen Sulfide Delivery from Caged-Carbonyl Sulfide Isomeric Donor Platforms. *J. Am. Chem. Soc.* **2017**, *139* (45), 16365−16376.

(18) Steiger, A. K.; Yang, Y.; Royzen, M.; Pluth, M. D. Bio-orthogonal "click-and-release" donation of caged carbonyl sulfide (COS) and hydrogen sulfide (H_2S). *Chem. Commun.* **2017**, *53* (8), 1378−1380.

(19) Steiger, A. K.; Marcatti, M.; Szabo, C.; Szczesny, B.; Pluth, M. D. Inhibition of Mitochondrial Bioenergetics by Esterase-Triggered COS/H_2S Donors. *ACS Chem. Biol.* **2017**, *12* (8), 2117−2123.

(20) Chauhan, P.; Bora, P.; Ravikumar, G.; Jos, S.; Chakrapani, H. Esterase Activated Carbonyl Sulfide/Hydrogen Sulfide (H2S) Donors. *Org. Lett.* **2017**, *19* (1), 62−65.

(21) Zhao, Y.; Steiger, A. K.; Pluth, M. D. Cysteine-activated hydrogen sulfide (H_2S) delivery through caged carbonyl sulfide (COS) donor motifs. *Chem. Commun.* **2018**, *54* (39), 4951−4954.

(22) Cerda, M. M.; Mancuso, J. L.; Mullen, E. J.; Hendon, C. H.; Pluth, M. D. Use of Dithiasuccinoyl-Caged Amines Enables COS/H_2S Release Lacking Electrophilic Byproducts. *Chem. - Eur. J.* **2020**, *26* (24), 5374−5380.

(23) Zhou, S. C.; Mou, Y. J.; Liu, M.; Du, Q.; Ali, B.; Ramprasad, J.; Qiao, C. H.; Hu, L. F.; Ji, X. Y. Insights into the Mechanism of Thiol-Triggered COS/H_2S Release from *N*-Dithiasuccinoyl Amines. *J. Org. Chem.* **2020**, *85* (13), 8352−8359.

(24) Gilbert, A. K.; Zhao, Y.; Otteson, C. E.; Pluth, M. D. Development of Acid-Mediated H_2S/COS Donors That Respond to a Specific pH Window. *J. Org. Chem.* **2019**, *84* (22), 14469−14475.

(25) Powell, C. R.; Foster, J. C.; Okyere, B.; Theus, M. H.; Matson, J. B. Therapeutic Delivery of H_2S via COS: Small Molecule and Polymeric Donors with Benign Byproducts. *J. Am. Chem. Soc.* **2016**, *138* (41), 13477−13480.

(26) Powell, C. R.; Kaur, K.; Dillon, K. M.; Zhou, M. J.; Alaboalirat, M.; Matson, J. B. Functional N-Substituted N-Thiocarboxyanhydrides as Modular Tools for Constructing H_2S Donor Conjugates. *ACS Chem. Biol.* **2019**, *14* (6), 1129−1134.

(27) Zhao, Y.; Bolton, S. G.; Pluth, M. D. Light-Activated COS/H_2S Donation from Photocaged Thiocarbamates. *Org. Lett.* **2017**, *19* (9), 2278−2281.

(28) Stacko, P.; Muchova, L.; Vitek, L.; Klan, P. Visible to NIR Light Photoactivation of Hydrogen Sulfide for Biological Targeting. *Org. Lett.* **2018**, *20* (16), 4907−4911.

(29) Sharma, A. K.; Nair, M.; Chauhan, P.; Gupta, K.; Saini, D. K.; Chakrapani, H. Visible-Light-Triggered Uncaging of Carbonyl Sulfide for Hydrogen Sulfide (H_2S) Release. *Org. Lett.* **2017**, *19* (18), 4822−4825.

(30) Levinn, C. M.; Steiger, A. K.; Pluth, M. D. Esterase-Triggered Self-Immolative Thiocarbamates Provide Insights into COS Cytotoxicity. *ACS Chem. Biol.* **2019**, *14* (2), 170−175.

(31) Chauhan, P.; Jos, S.; Chakrapani, H. Reactive Oxygen Species-Triggered Tunable Hydrogen Sulfide Release. *Org. Lett.* **2018**, *20* (13), 3766−3770.

(32) We also prepared the S-alkyl analogue of MeTCM-Me, but failed to observe H_2S release from this compound. See Scheme S1 and Figure S40.

(33) Siegel, L. M. A Direct Microdetermination for Sulfide. *Anal. Biochem.* **1965**, *11* (1), 126.

(34) Frisch, M. J.; Trucks, G. W.; Schlegel, H. B.; Scuseria, G. E.; Robb, M. A.; Cheeseman, J. R.; Scalmani, G.; Barone, V.; Mennucci, B.; Petersson, G. A.; Nakatsuji, H.; Caricato, M.; Li, X.; Hratchian, H. P.; Izmaylov, A. F.; Bloino, J.; Zheng, G.; Sonnenberg, J. L.; Hada, M.; Ehara, M.; Toyota, K.; Fukuda, R.; Hasegawa, J.; Ishida, M.; Nakajima, T.; Honda, Y.; Kitao, O.; Nakai, H.; Vreven, T.; Montgomery, J. A., Jr.; Peralta, J. E.; Ogliaro, F.; Bearpark, M.;

Heyd, J. J.; Brothers, E.; Kudin, K. N.; Staroverov, V. N.; Kobayashi, R.; Normand, J.; Raghavachari, K.; Rendell, A.; Burant, J. C.; Iyengar, S. S.; Tomasi, J.; Cossi, M.; Rega, N.; Millam, J. M.; Klene, M.; Knox, J. E.; Cross, J. B.; Bakken, V.; Adamo, C.; Jaramillo, J.; Gomperts, R.; Stratmann, R. E.; Yazyev, O.; Austin, A. J.; Cammi, R.; Pomelli, C.; Ochterski, J. W.; Martin, R. L.; Morokuma, K.; Zakrzewski, V. G.; Voth, G. A.; Salvador, P.; Dannenberg, J. J.; Dapprich, S.; Daniels, A. D.; Farkas, Ö.; Foresman, J. B.; Ortiz, J. V.; Cioslowski, J.; Fox, D. J. *Gaussian 09*, Revision D.02; Gaussian, Inc.: Wallingford, CT, 2009.

(35) Kumar, M.; Francisco, J. S. Hydrogen Sulfide Induced Carbon Dioxide Activation by Metal-Free Dual Catalysis. *Chem. - Eur. J.* **2016**, *22* (13), 4359−4363.

(36) The impact of N-alkylation on the rotational barrier of the anionic thiocarbamate was investigated across a suite of N−H, N−Me, and N−indoline thiocarbamate donors. N-alkylation impacts this rotational barrier, but the rotational barriers do not correlate with COS release profiles. See the Supporting Information.

(37) Jessen, H. J.; Schulz, T.; Balzarini, J.; Meier, C. Bioreversible Protection of Nucleoside Diphosphates. *Angew. Chem., Int. Ed.* **2008**, *47* (45), 8719−8722.

https://doi.org/10.1021/acs.joc.0c02778
J. Org. Chem. 2021, 86, 5443−5451